RESEARCH ARTICLE

A turbulent boundary layer over a two-dimensional rough wall

Lyazid Djenidi · Robert A. Antonia ·
Muriel Amielh · Fabien Anselmet

Abstract Particle image velocimetry (PIV) measurements and planar laser induced fluorescence (PLIF) visualizations have been made in a turbulent boundary layer over a rough wall. The wall roughness consisted of square bars placed transversely to the flow at a pitch to height ratio of $\lambda/k = 11$ for the PLIF experiments and $\lambda/k = 8$ and 16 for the PIV measurements. The ratio between the boundary layer thickness and the roughness height k/δ was about 20 for the PLIF and 38 for the PIV. Both the PLIF and PIV data showed that the near-wall region of the flow was populated by unstable quasi-coherent structures which could be associated to shear layers originating at the trailing edge of the roughness elements. The streamwise mean velocity profile presented a downward shift which varied marginally between the two cases of λ/k, in agreement with previous measurements and DNS results. The data indicated that the Reynolds stresses normalized by the wall units are higher for the case $\lambda/k = 16$ than those for $\lambda/k = 8$ in the outer region of the flow, suggesting that the roughness density effects could be felt well beyond the near-wall region of the flow. As expected the roughness disturbed dramatically the sublayer which in turn altered the turbulence production mechanism.

L. Djenidi (✉) · R. A. Antonia
School of Engineering, University of Newcastle,
Newcastle, Australia
e-mail: lyazid.djenidi@newcastle.edu.au

R. A. Antonia
e-mail: robert.antonia@newcastle.edu.au

M. Amielh · F. Anselmet
IRPHE, Marseille, France
e-mail: amielh@irphe.univ-mrs.fr

F. Anselmet
e-mail: fabien.anselmet@irphe.univ-mrs.fr

The turbulence production is maximum at a distance of about $0.5k$ above the roughness elements. When normalized by the wall units, the turbulence production is found to be smaller than that of a smooth wall. It is argued that the production of turbulence is correlated with the form drag.

1 Introduction

There has recently been a renewal of interest in rough wall flows (see Jimenez 2004 for a latest comprehensive review on rough wall studies), largely made possible by the improvement of measurement techniques and direct numerical simulations, which opens up new perspective on the subject. Indeed, the relatively slow progress that has been made in understanding how the roughness affects the turbulence structure reflects, by and large, the extra parameters involved, by comparison to the smooth wall case, and the general difficulty of making reliable measurements in the vicinity of a rough surface. With the development of laser Doppler velocimetry (LDV) technique and particle image velocimetry (PIV), for example, more reliable data can be obtained in the vicinity of the rough wall. Yet, difficulties still persist in particular with three-dimensional (3-D) roughnesses. In the present work we focus on a 2-D rough wall, made of transverse square bars. While such roughness differs significantly from 3-D roughnesses, it nevertheless allows a simplified study and has important applications, often used to enhance mass and heat transfer.

Turbulent flows over a 2-D rough such as studied here, have been the subject of many investigations since the pioneering work of Perry et al. (1969). For example, Djenidi et al. (1999) reported Laser Doppler Velocimetry

(LDV) measurements and flow visualizations (with the PLIF technique) for a turbulent boundary layer over a surface consisting of square bars (height k = width w) attached to the wall where the steamwise pitch λ is equal to $2k$ (λ is the streamwise separation between two consecutive roughness elements). The use of LDV and PLIF techniques proved to be quite helpful in gaining insight into the near-wall flow organization. In particular, they helped confirm and extend the earlier observations by Townes and Sabersky (1966) over the same surface. For instance, they vividly showed that fluid ejections from the flow in the cavity (space between two consecutive roughness elements) into the overlying flow took place randomly and that these ejections were associated with the passage of near-wall quasi-streamwise vortices, similar to those found in a smooth wall turbulent boundary layer. Most recently, further progress on this type of rough walls has been made with the use of direct numerical simulations (DNSs, Leonardi et al. 2003; Ikeda and Durbin 2007; Ashrafian et al. 2004; Kogstad et al. 2005) and large eddy simulations (LESs, Cui et al. 2003). Such studies highlighted how the near-wall local properties of the flow can be dramatically altered and controlled by the roughness. It must be stressed though that all these simulations have been carried out for turbulent channel flows with a relatively low Reynolds number. This in itself is not too worrisome given that the form drag is the dominant contributor to the total drag under fully rough conditions. However, there is the possibility that differences exist, at least in the outer region, between channel flows and boundary layers. It is therefore important to study turbulent boundary layers over 2-D rough walls. Another important issue that needs to be looked at is the influence of the ratio k/H or k/δ (H and δ are the channel half-height and the boundary layer thickness, respectively). In most experimental and DNS studies, the ratio k/H (k/δ) may not be small enough to neglect the blockage effect. Jimenez (2004) recommends that this ratio to be equal or less than 0.025 to ensure that roughness does not perturb more than 50% of the logarithmic layer.

This paper reports particle image velocimetry (PIV) and planar laser induced fluorescence (PLIF) measurements in a turbulent boundary layer over a wall on which 2-D square bars are attached with a pitch to height ratio of λ/k = 8, 11 and 16. In the case of the PIV measurements, the ratio k/δ is 0.026. Also the Reynolds number based on the momentum thickness is about 5,300 for the PIV measurements, which minimizes any possible low Reynolds number effects on the results. The main objective of the study is to assess the rough wall effects on the flow with these relatively adequate laboratory flow conditions (low k/δ and high Reynolds numbers). The present work is part of a more extensive programme aimed at studying in detail a rough wall boundary layer with variable λ/k.

2 Experimental setup

Two complementary experiments were carried out in two different water tunnels, one at Newcastle (Australia) for the PLIF visualizations, and the other at Marseille (France) for the PIV measurements.

2.1 The rough wall

The rough wall consisted in a series of stain steel square bars ($k = w$) fixed to a flat plate and spanning the full width of the plate, with a separation between the corresponding points of two consecutive bars λ (Fig. 1). For the experiments at Newcastle, k = 3 mm and λ = 33 mm, while k = 4 mm and λ = 32 and 64 mm at Marseille. In the following presentation of the results, the origin $x = 0$ (x is the distance in the streamwise direction) is chosen to be at the trailing edge of a roughness element, while $y = 0$ (y is distance in normal to the wall direction) is at the base of the roughness element along the bottom wall (see Figs. 1, 2).

2.2 PLIF setup

The PLIF visualizations were made in a constant-head closed circuit vertical water tunnel with a 2 m long square (250 mm × 250 mm) Perspex test section. One of the working section walls was used as the rough wall. The boundary layer was tripped with 4.5 mm high pebbles glued over the wall span and 30 mm upstream of the first roughness element (Fig. 2). The roughness elements extended over a streamwise distance of 1.8 m downstream of the trip. Detailed flow visualizations were made at a distance of 1 m downstream of the first element; at this location, the boundary layer thickness δ was about $20k$. The Reynolds number R_θ based on the momentum thickness θ (θ was estimated midway between two roughness elements), was approximately 2,100. While this is not a very high Reynolds number, the value is high enough to ensure that the results are weakly affected by the low Reynolds number effects. Note also that low Reynolds number effects are less effective in a rough surface turbulent boundary layer than in a smooth wall
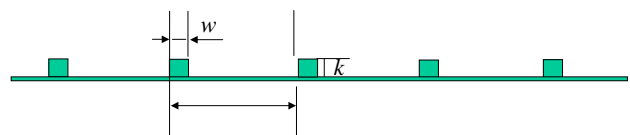

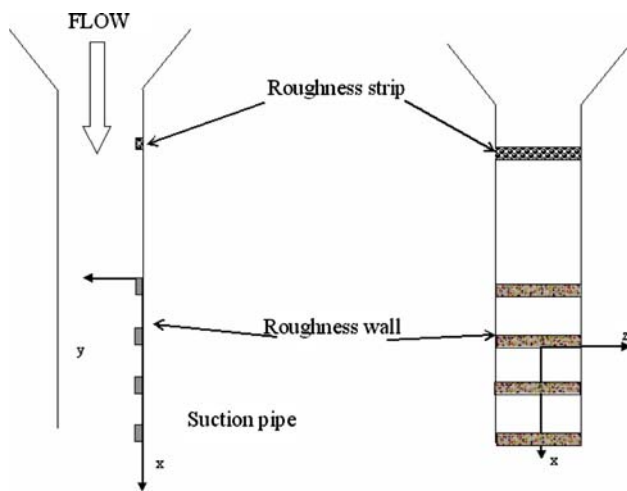**Fig. 1** Side view schematic representation of the two-dimensional rough wall with dimension definitions

Fig. 2 Sketch of the rough wall mounted in the water tunnel at Newcastle (Australia)

Fig. 3 Water channel "Herode" at Marseille (France)

one, particularly, as in the present case, when the form drag is the most dominant contributor to the total drag. The freestream turbulence intensity was about 5%.

To implement the PLIF method, fluorescein dye was injected through a transverse slit (0.25 mm × 240 mm) machined flush with the wall at a distance of about $2k$ downstream of a roughness element. The dye was injected continuously using a small pump at a flow rate low enough to avoid any perturbations to the flow. A 4 W multimode Argon-Ion laser was used as a light source (≈ 2 W) for the PLIF. The reflection of the laser beam onto a cylindrical mirror caused the expansion of the beam into a planar light sheet. The 250 μm thick light sheet was placed either parallel or normal to the wall so as to enable views in either the $(x$–$y)$ or $(x$–$z)$ plane (z is the spanwise direction). The flow visualization images were recorded via a CCD camera onto a video tape and then digitized through a video card (256 grey levels). Additional details on the experiment facility can be found in Djenidi et al. (1999) and Rehab et al. (1999). The roughness element located at about 1 m ($30k$) downstream of the trip is taken as the reference for the x distance.

2.3 PIV setup

The PIV measurements were carried out in an open water channel ("Herode"). The test section was 8 m long, 60 cm wide and 60 cm deep (Fig. 3). The 2 m long rough wall, commenced at a distance of 5 m downstream of the contraction. A 200 mJ pulsed Nd:Yag was used to illuminate the flow. The laser sheet was shot from the top through a 10 cm diameter Perspex porthole. The porthole was flush with the free surface in order not to disturb the flow. A set
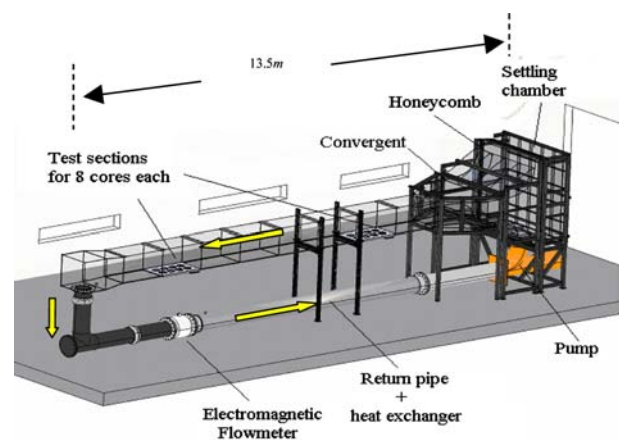
of cylindrical lenses converted the laser light into a vertical thin sheet located at the mid-plane ($z = 0$) of the channel. A digital camera (Kodak ES 1.0) was used with a charge-coupled device (CCD) ($1,008 \times 1,008$ pixels). The PIV images were post-processed using the adaptive-correlation method (FlowManager 4.30.27; Dantec Dynamics) to obtain the instantaneous velocity fields. Each image, which corresponded to an area of about 6 cm × 6 cm of the actual flow, was subdivided into 64×32 pixels with 50% overlap. Tests were made with 32×32 resolution and no discernable differences were observed with the 64×32 resolution indicating that the uncertainties associated with the spatial resolution were small and did not affect the results. Thus, the latter resolution was adapted as it allowed faster data processing. About 1,500 velocity fields were used to obtain the statistical results such as the mean velocity and the Reynolds stress profiles for all flow configurations. This number of samples was found to be enough to obtain convergence for the mean velocity and Reynolds stresses. Each profile was composed of four segments, obtained by moving the camera in the y direction. An overlap of 1 cm was allowed between successive segments permitting to reconstruct the entire velocity field. The matching between two segments was carried out by matching the mean velocity profiles.

The water was seeded with particles (Optimage Ltd) with an average size of 30 μm and a specific gravity of 1.0 ± 0.02. These particles were polycrystalline in structure and provided a high light-scattering efficiency (five times greater than latex spheres which have a similar refractive index). The water depth ($h = 50$ cm) and the flow rate (250 m^3/h) were kept constant. The free surface was relatively calm with no waves occurring at the surface. The freestream longitudinal and wall-normal intensities were about 7.0% and the boundary layer thickness was almost half of the size of the water depth. The Reynolds

number R_θ was about 5,320 half way through the rough wall, where the measurements have been made. This ensures that low Reynolds number effects are negligible, or at least minimize, and should not affect the generality of the results. The ratio δ/k was about 38, about the lower limit for neglecting the blockage effect of the roughness elements on the flow (Jimenez 2004).

3 Results

3.1 PLIF measurements

Figure 4 shows an example of instantaneous pictures of the near-wall flow between consecutive roughness elements. The figure implies the existence of a shear layer, which develops at the tip of the roughness element. It should be noted that this shear layer develops within a turbulent environment. The interaction between this local shear layer and the overlying flow is still not clearly understood. Associated with the shear layer, there are coherent structures similar to those observed in a plane mixing layer and with a streamwise length scale of the order of the roughness height, k and a wavelength of about $2k$. There is a small recirculatory zone (Fig. 4c)
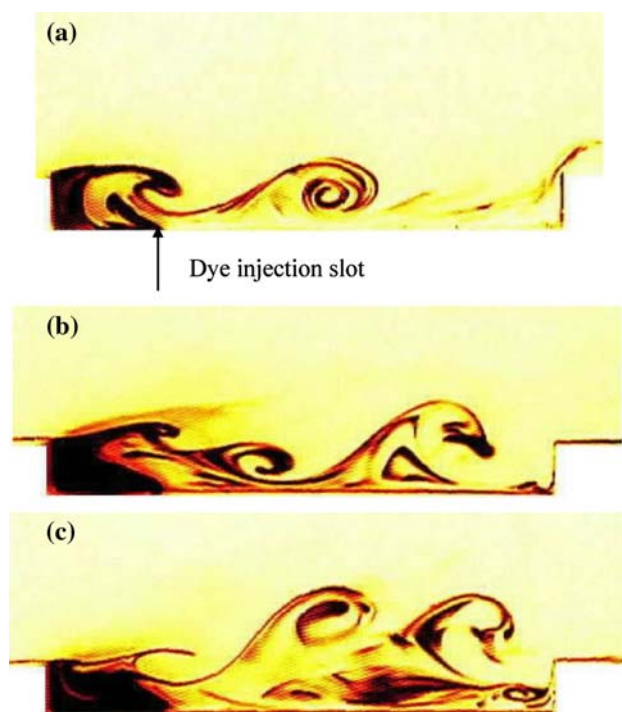

Fig. 4 A series of $(x–y)$ plane views of the near-wall flow. The flow is from *left* to *right*. The actual ratio λ/k is respected in this presentation

immediately upstream of the consecutive element. This recirculatory motion is intermittent due certainly to the flapping of the shear layer.

The flow for $\lambda/k = 11$ is quite different from that observed when $\lambda/k = 2$ (Perry et al. 1969; Leonardi et al. 2004), at least in the near-wall region. In this latter case, the recirculatory motion occupied the whole cavity and was only partly destroyed when fluid escaped from the cavity (Perry et al. 1969). This clearly highlights the structural differences in the near-wall region between the two rough surfaces, and also explains the large difference in the form drag between the two surfaces (Townes and Sabersky 1966). While the case $\lambda/k = 2$ has little form drag, the case $\lambda/k = 11$ has a quite large one. The DNS of Leonardi et al. (2003) and the experiments of Kameda et al. (2004) in a turbulent boundary layer over square rob rough wall showed that the form drag is maximum when $\lambda/k = 8$.

The structures associated with the shear layer present a particularly high degree of coherence. The overlying turbulent flow transports these structures without, seemingly, disrupting their evolution. The manner in which these structures interact with the roughness elements is not trivial. The vertical length scale of the structures is of order k, suggesting that they are likely to dominate the flow in this region. In that respect, they may play an important role in terms of transporting momentum and scalar quantities. These structures are also an additional source of turbulent energy generation which is likely to contribute to the enhancement of the turbulence mixing near the wall. To our knowledge, no information exists on the interaction between the shear layer and the overlying turbulent boundary layer. This is worthy of further investigation.

One may infer from Fig. 4 that the flow in the near-wall region is dominated by 2-D structures. However, the $(x–z)$ plane view of Fig. 5 reveals that this is not the case. The dye is concentrated within unsteady localized regions in the
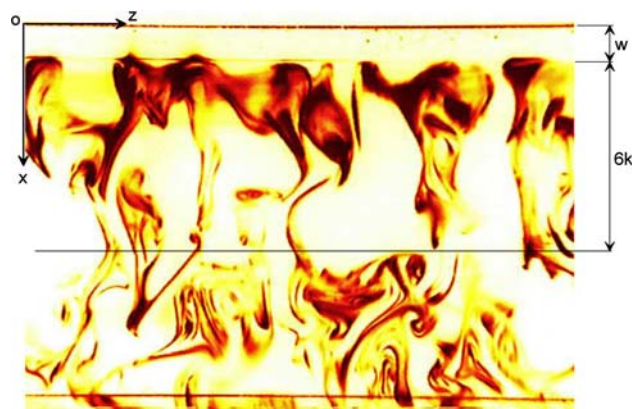

Fig. 5 A $(x–z)$ plane view at $y = k$. The flow is from *top* to *bottom*

spanwise direction near the injection point from where it is entrained downstream. There is a clear demarcation along the spanwise direction in the dye distribution: in the region $0 < x/k \leq 6$, the dye appears to be concentrated into elongated narrow regions with a spanwise spacing of about 2–$3k$. In the region $x/k \geq 6$, the dye is patchy, suggesting a strong three-dimensionality of the flow. The demarcation "line" may correspond to the reattachment line. It is not yet clear whether the elongated streaky structures observed in the region $0 < x/k < 6$ are reminiscent of the low-speed streaks observed when $\lambda/k = 2$ (Perry et al. 1969) or of those for a smooth wall. However, flow visualization sequences in the $(x$–$z)$ plane did not reveal mushroom-like structures, usually interpreted as cross-sectional views of low-speed streaks. This suggests that there is no low-speed streaks when λ/k equals to 11 and supports the idea that the mechanism of turbulence production for this case is different from that of $\lambda/k = 2$ and a smooth wall.

3.2 PIV measurements

While the results of the PLIF experiment show interesting results one should keep in mind the value of the ratio δ/k which is about 20. This is half the lower limit recommended by Jimenez (2004). To try to overcome this limit, PIV measurements were carried out where $\delta/k = 38$ could be achieved.

3.2.1 Mean streamlines

Figure 6 shows some time averaged streamlines between and immediately above the roughness elements for $\lambda/k = 8$ and 16. The figure provides a qualitative description of the near-wall mean flow. Notice that in the case of $\lambda/k = 8$, the streamlines are not properly defined just behind the second roughness element due to a poor lighting of this region (the laser light source was located at a x-position so that the laser light sheet illuminates the full region between the first two roughness elements shown in the figure). In both cases of λ/k a similar flow type is observed. The figure presents similar features to those observed in the DNS of Leonardi et al. (2003) and Ikeda and Durbin (2007). The streamlines indicate a flow separation occurring at the trailing edge of the roughness elements and a well-defined recirculation region behind the roughness. The recirculation centre is at about $2.0k$ behind the roughness element and at $y = 0.5k$. The flow then reattaches at the wall between two elements. The reattachment point is at about $3.5k$ and $4.2k$ for $\lambda/k = 8$ and 16, respectively. This is smaller than the location of the demarcation line shown in Fig. 5, suggesting that this latter may not represent the reattachment point as initially
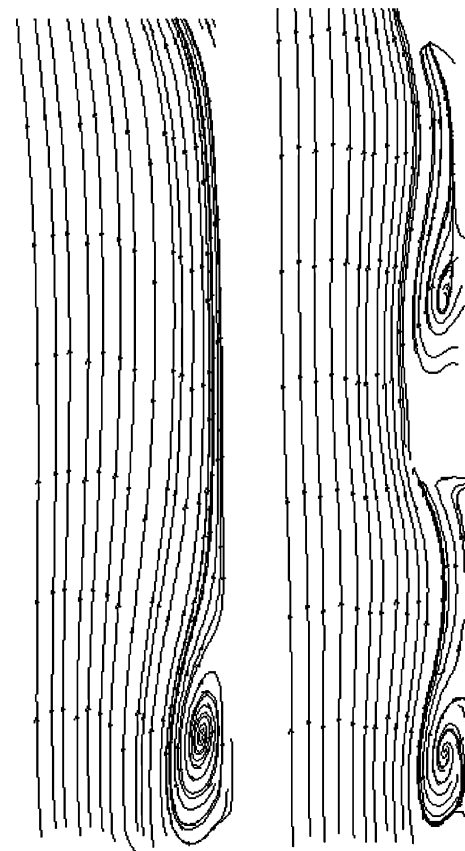

Fig. 6 Time averaged two-dimensional streamlines. *Top* $\lambda/k = 16$; *bottom* $\lambda/k = 8$

thought. After the reattachment, the streamlines lift up as they approach the next roughness element. While not visible here because of the relatively low resolution of the PIV measurements, the streamlines suggest that a secondary vortex takes place at each corners of the roughness elements, as observed in the DNS of Leonardi et al. (2003) and measurements of Kameda et al. (2004); these vortices are of opposite direction.

3.2.2 Mean flow

Figures 7 and 8 show the distributions of the mean streamwise velocity U/U_e and the normal velocity fluctuations u'/U_e and v'/U_e (the prime denotes the rms) for various x positions between two consecutive roughness elements for $\lambda/k = 8$ and 16. Noting that no smoothing has been applied to the data, it is assuring to observe that the scatter in the data is almost negligible. This indicates that the uncertainties related to spatial resolution and (time) convergence are small. There are though some apparent discontinuities in the mean velocity and Reynolds stress profiles (in particular in the v' profiles). They occur in the

Fig. 7 Time averaged
streamwise velocity profiles at
various *x*-locations. *Left*
*λ/k* = 16; *right λ/k* = 8
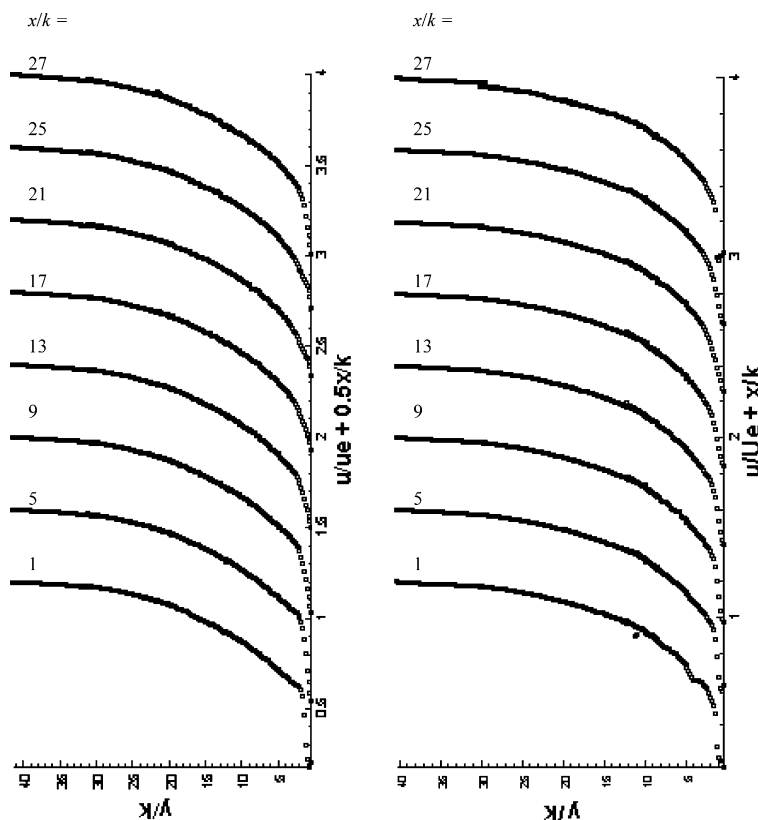
overlap regions between two segments of the velocity field. These discontinuities are likely to reflect a slight misalignment of the vertical axis of the camera with the *y*-direction of the wall. It seems that the measurements of *v′* is more affected than *u′* and *U* by this misalignment.

One can observe a streamwise variation in all the distributions in the near wall region. Note that a local peak near the wall is observed in some u'/U_e and v'/U_e distributions behind the roughness element. The variation for U/U_e vanishes when $y/k > 5$ and 9 for $\lambda/k = 8$ and 16, respectively. The variation also disappears in u'/U_e and v'/U_e but at a shorter distance from the wall ($y/k < 3$–4; this is also seen in the Reynolds shear stress, $<uv>$). The collapse of the distributions is well visible when the distributions are plotted without shift (not show here). The observation that the streamwise variation in u'/U_e and v'/U_e distributions vanishes nearer to the wall than in the U/U_e profile illustrates the fact that the turbulent field responds and adapts faster than the mean flow to a change in the wall geometry. For an analysis purpose the collapse of the distribution at a distance less *y* than $10k$, may justify a space averaging over a distance λ, particularly since the streamwise variation of δ is negligible over such a distance as shown in Fig. 7. All subsequent quantities presented are time and space (over λ) averaged.

Figure 9 shows the PIV mean distributions U^+ and u'^+ (where the superscript sign + denotes normalizing with the

friction velocity, u_τ, and the viscosity, *v*) for the case $\lambda/k = 16$ with laser Doppler measurements (LDV) data for a smooth wall turbulent boundary layer. The later were taken in the same water channel where the PIV measurements were made but without the roughness elements. The bottom plots of Fig. 9 are the u'^+ at a larger scale and where a smoothening has been applied to the LDV data for attenuating the scattering effect. The friction velocity for the LDV was estimated using the Clauser method while the DNS results of Leonardi et al. (2003) and experimental data of Kameda were used to deduce the values of u_τ for the PIV measurements. A third method (Kogstad and Antonia 1999; Furuya et al. 1976) was also used to estimate u_τ for the rough wall, which consists in taking the magnitude $-<uv>_{plateau}$ as u_τ^2; $-<uv>_{plateau}$ is the value of the plateau observed in the $<uv>$ distributions (see Smalley et al. 2001 for discussion on this method). The use of Clauser method for the smooth wall can be justified since R_θ is about 5,300 which allows for the presence of a well defined log region in the mean velocity profile. In the case of the rough walls, the problem is a more complicated because the velocity profile is affected by the roughness, through two additional unknown variables in the log law, the virtual origin, and the roughness function ΔU^+ (a shift in the velocity profile with respect to that of a smooth wall). The DNS of Leonadi et al. (2003) in a channel flow with transverse square bars on one wall revealed that the

Fig. 8 Time averaged profiles
of the turbulence intensities at
various *x*-locations. **a**, **c**
$\lambda/k = 16$; **b**, **d** $\lambda/k = 8$. **a**,
b u'/U_e; **c**, **d** v'/U_e
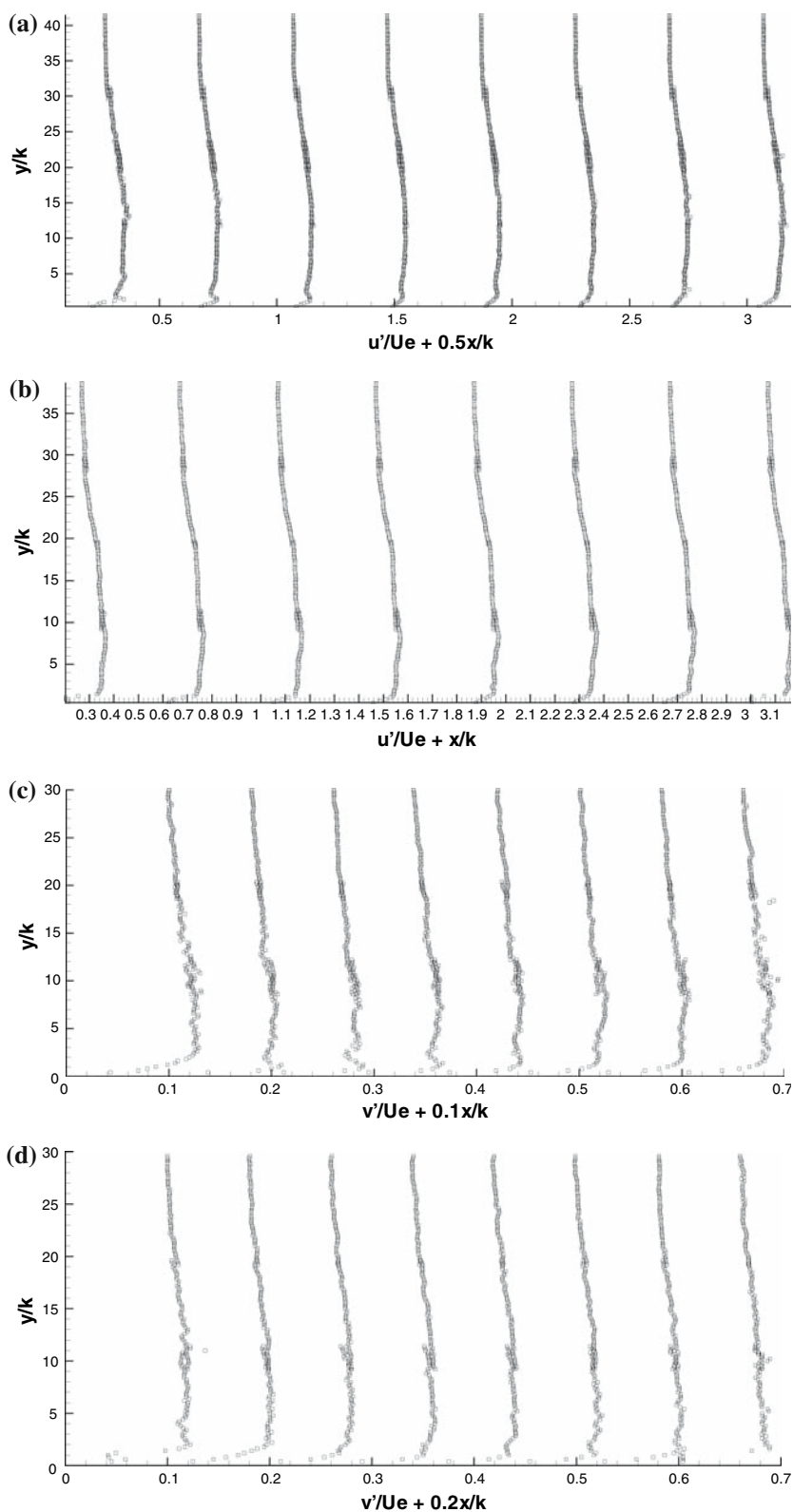
roughness function ΔU^+ is a function of λ/k and follows closely the form drag variation with λ/k. Kameda et al. (2004) measurements in a turbulent boundary over square

bars similar to the present ones showed that the form drag follows that of the DNS of Leornardi et al. (2003) relatively well. These observations suggest, at least for the
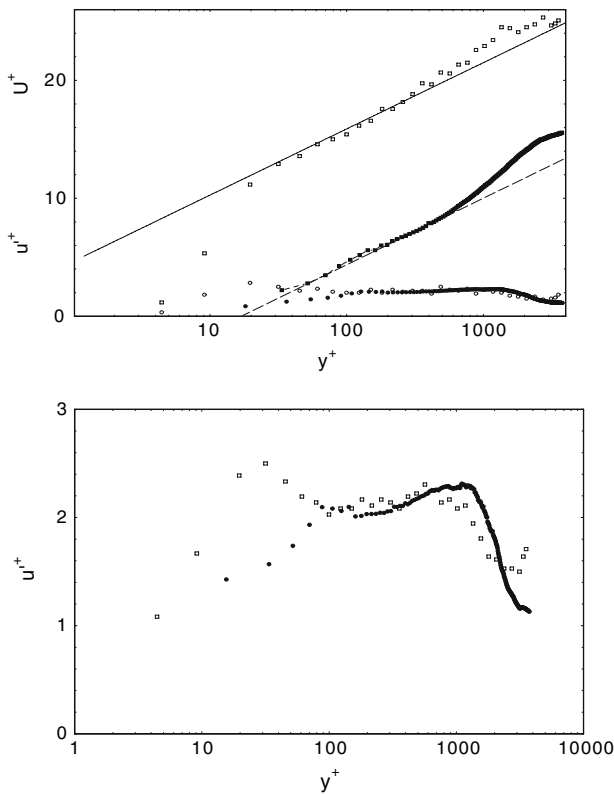
Fig. 9 Streamwise mean velocity and velocity fluctuations (rms) profiles. *Open symbols* smooth wall (LDV); *closed symbols* rough wall $\lambda/k = 16$. *Bottom* streamwise velocity fluctuations (rms) profiles of *top* plot but at a larger plot scale. (LDV data $\delta = 17$ cm, $\theta = 1.7$ cm, $U_e = 0.3$ m/s, $u_\tau = 0.012$ m/s)

square bar roughness, that both the drag force and ΔU^+ depend mainly on the ratio λ/k and are less sensitive to k/δ and the Reynolds number. This of great interest here since one can obtain the values of the drag force from the DNS of Leonardi et al. (2003) and determine the values of u_τ and ΔU^+ for the present rough walls; this method is used here to estimate u_τ and ΔU^+. Table 1 below presents the values of both ΔU^+ and u_τ for the two cases of λ/k.

The table also includes the friction velocity estimated using the third method as defined above. It is interesting to observe that the value of the friction velocity from both methods are consistent (the ratio $u_{\tau(\Delta U)}/[-\langle uv \rangle_{\text{plateau}}]^{1/2}$ is about 1.1 and 1.088 for $\lambda/k = 8$ and 16, respectively). Values of $[-\langle uv \rangle_{\text{plateau}}]^{1/2}$ were used for normalizing the

Table 1 Roughness function and friction velocity

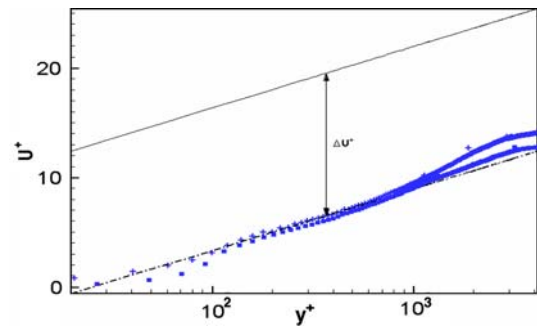| λ/k	ΔU^+	u_τ (m/s)	
		u_τ	$[-\langle uv \rangle_{\text{plateau}}]^{1/2}$
8	13.3	0.022	0.020
16	12.9	0.0198	0.0182

Fig. 10 Streamwise mean velocity profiles. *Plus* $\lambda/k = 16$, *filled square* $\lambda/k = 8$

data in all subsequent figures. In Fig. 9 (and later in Fig. 10) the virtual origin is take at $y = 0.25k$ and $0.5k$ for $\lambda/k = 16$ and 8, respectively, following the results of Leornadi et al. (2003). Note though that such small values will not have a big impact on the plots of the mean velocity since the portion of the log region is at least as twice larger than k^+. As expected the rough wall velocity profile exhibits a downward shift with respect to the smooth wall velocity distribution. The value of ΔU^+ for the DNS data of Leonardi et al. is about 12 and 11.3 for $\lambda/k = 8$ and 16, respectively. While these values differ from that of Table 1 they show a similar trend, i.e., a decrease with increasing λ/k.

The profile for u'^+ over the rough wall differs from that of the smooth wall for $y^+ \leq 90$. The disappearance of the local peak in u'^+ over the rough wall indicates the dominance of the form drag over the viscous one, as observed in Leonardi et al. (2003) and Kameda et al. (2004) for example. The two distributions present a similar trend for $y^+ > 120$ ($y/\delta > 0.03$); both distributions develop a maximum. The rough wall data depart significantly from those of the smooth wall for $y^+ > 700$. This later observation is to be taken with care as the value of u_τ is critical here. PIV measurements need to be carried out in the turbulent boundary layer in the water tunnel without roughness and the same method used to estimate the friction velocity before conclusive information can be drawn.

Figures 10 and 11 (only every second point is presented in Fig. 11 for clarity; also in that figure and subsequent ones, the y-origin is taken at the base of the roughness elements) show the distributions of U^+, u'^+, v'^+ and $\langle u^+v^+ \rangle$ for both cases of λ/k. The downward shift ΔU^+ in the velocity profile for $\lambda/k = 16$ ($\Delta U^+ = 11.85$) is slightly less than that for $\lambda/k = 8$ ($\Delta U^+ = 12.1$). This is consistent with the results of Leonardi et al. (2003) and Furuya et al. (1976), which showed that ΔU^+ is maximum for λ/k around 8. Quite interestingly, the present values of ΔU^+ (obtained from Fig. 10) are similar to those of Furuya et al. (1976).

The distributions of u'^+ and v'^+ show moderately high values in the most outer part of the boundary layer which
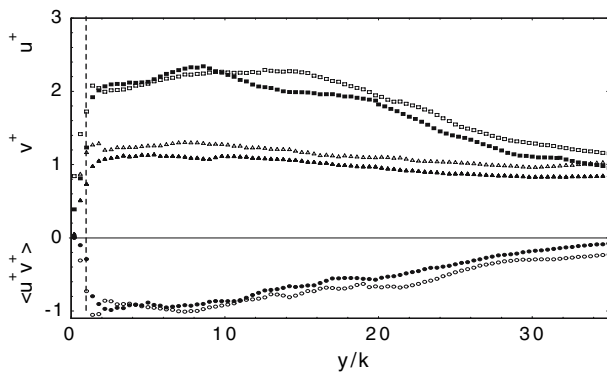
Fig. 11 Reynolds stresses profiles. *Open symbols* $\lambda/k = 16$, *closed symbols* $\lambda/k = 8$

Fig. 13 Coefficient of correlation. *Open symbols* $\lambda/k = 16$, *closed symbols* $\lambda/k = 8$

reflects a relatively elevated level of background turbulence within the tunnel. In the case of $\lambda/k = 16$, all the distributions show a small local peak just above the roughness crest plane, $y/k = 1$; no such local peak is observed for $\lambda/k = 8$. It indicates a local increase in the turbulence intensity for $\lambda/k = 16$ when compared to the case for $\lambda/k = 8$. There are some differences in the distributions between the two cases of λ/k. The values of u'^{+}, v'^{+} and $-\langle u^{+}v^{+}\rangle$ when $y/k > 10$ are systematically higher for the larger ratio λ/k than those for the smaller one, possibly suggesting that the change in the roughness density is felt well into the boundary layer. Note that v'^{+} remains higher for $\lambda/k = 16$ well below the line $y/k = 1$, illustrating the fact that v' is more sensible than u' to the wall geometry. It is however rather surprising to observe that both u'^{+} and $-\langle u^{+}v^{+}\rangle$ do not seem to be much different for $y/k < 10$ between $\lambda/k = 8$ and 16. The differences in u'^{+}, v'^{+} between the two cases of λ/k is further assessed when the ratios v'^{+}/u'^{+} are compared (Fig. 12). The data for $\lambda/k = 8$ are consistently lower that those of $\lambda/k = 16$, with a larger difference in the region close to the wall ($0 < y/k < 10$).
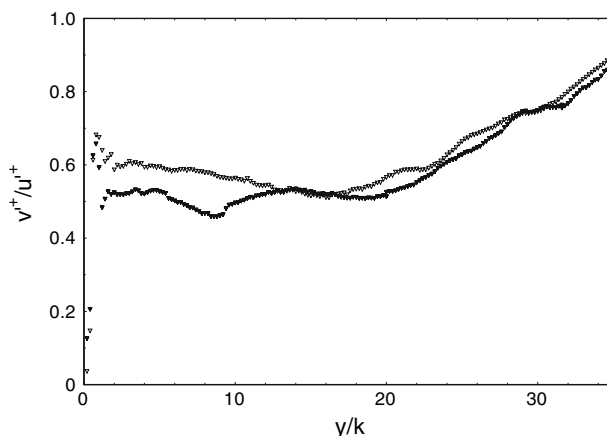
Also, the coefficient of correlation $-\langle uv\rangle/u'v'$ (Fig. 13) is larger for $\lambda/k = 8$ than $\lambda/k = 16$ in the region $0 < y/k < 15$, but almost no difference is observed for $20 < y/k < 30$. Above $y/k = 30$ the data for $\lambda/k = 8$ become smaller than those for $\lambda/k = 16$. Whether this latter feature is real or not is not clear yet. Altogether the data of Figs. 11, 12 and 13 would suggest that the effects of the rough wall are felt well into the boundary layer, at least for this type of roughness.

3.2.3 Turbulence production

The normalized turbulence production term $-\langle u^{+}v^{+}\rangle\partial U^{+}/\partial y^{+}$ is shown in Fig. 14 for both $\lambda/k = 8$ and 16. Strong production is observed just above the roughness, with a peak at $y/k = 1.55$ and 1.45 for $\lambda/k = 8$ and 16, respectively. The production is also maximum near the wall in a smooth wall turbulent boundary layer. DeGraaff and Eaton (2000) showed in a smooth wall turbulent boundary layer that the maximum of $-\langle u^{+}v^{+}\rangle\partial U^{+}/\partial y^{+}$ is about 0.25 for

Fig. 12 Ratio v'/u'. *Open symbols* $\lambda/k = 16$, *closed symbols* $\lambda/k = 8$
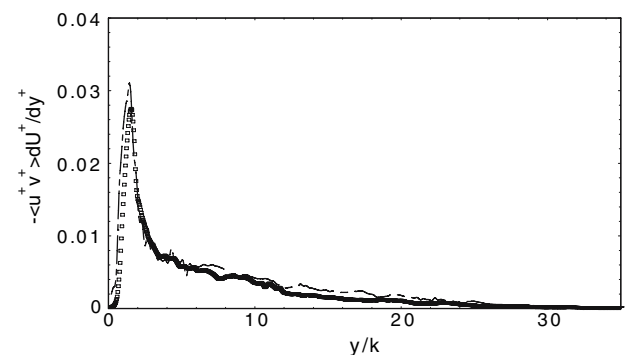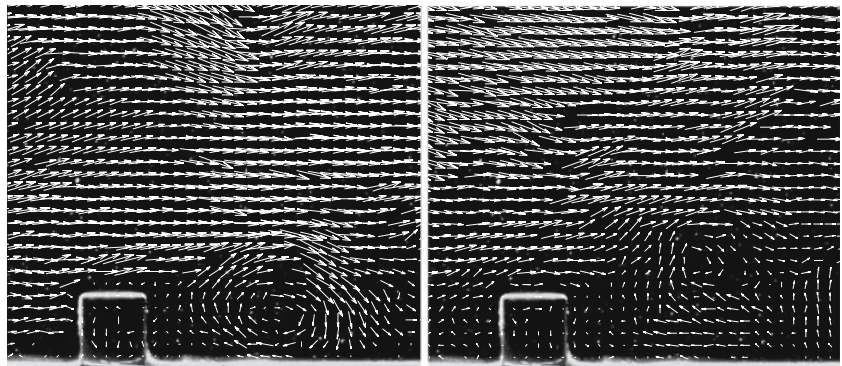

Fig. 14 Turbulence production $-\langle uv\rangle\partial U/\partial y$. *Dashed line* $\lambda/k = 16$, *symbols* $\lambda/k = 8$

Fig. 15 Two instantaneous velocity field around a roughness element for $\lambda/k = 16$

$R_\theta = 5{,}200$. This is about ten times larger then the present values measured here. They also show that the maximum occurs at the y location where $-\langle u^+ v^+ \rangle = 0.5$ ($y^+ = 10$). In the present flow conditions, the maximum of production occurs at y for which $-\langle u^+ v^+ \rangle$ is about 0.87 and 1 for $\lambda/k = 8$ and 16, respectively. In the smooth wall turbulent boundary layer, production is related to the dynamics of the near-wall quasi-coherent longitudinal vortices (Panton 1999) and reflects strong viscous effects. As seen from the PLIF images earlier, there are no longitudinal vortices here. The roughness elements disturb dramatically the sublayer causing a different mechanism for the turbulence production over the present rough wall. The higher value of the production peak for $\lambda/k = 16$ (14% higher) as compared to $\lambda/k = 8$ indicates that the viscosity effects are more important in the former case than the latter. The DNS data of Leonardi et al. (2003) show that the viscous drag is minimum at $\lambda/k = 8$ while the form drag is maximum. Possibly, one could correlate the production of turbulence with the form drag (or the viscous drag). Thus, the relatively small level of (wall unit normalized) turbulence production in the near wall region would explain the lower values of u'^+ relative to its smooth wall counterpart, as shown in Fig. 9, despite the high drag caused by the roughness. Quite interesting, the profile of u'^+ on the rough wall suggests that the mechanism of energy transfer between the individual components of the turbulent kinetic energy is also altered by the roughness. In the outer region of the boundary layer, the level of turbulence production for $\lambda/k = 16$ appears to be higher than that for $\lambda/k = 8$.

3.2.4 Vortical structures

The PLIF measurements revealed that quasi-coherent structures in the form of spanwise vortices take place in the wall region. Such structures are also visible in the PIV data. Figure 15 shows two instantaneous velocity fields in the region of a roughness element for $\lambda/k = 16$ (the instantaneous velocity fields for $\lambda/k = 8$ present comparable features to the case $\lambda/k = 16$). The figure shows a remarkable similarity to the PLIF data. In the left plot of Fig. 15, a vortical structure is located at about $x/k = 2$ and $y/k = 1$ while on the right plot the center of the vortical structure is roughly at $x/k = 2.5$ and $y/k = 1.5$. A time sequences of PIV images show that these structures are convected downstream and, as Fig. 15 indicates, pushed downward or upward. Also the sequence revealed that these structures are quickly deformed and destroyed as compared to the PLIF data. The reason is likely to be related to a stronger turbulence activity in the case of the PIV measurements where the R_θ is about 2.5 times larger than that of the PLIF measurements. Ikeda and Durbin (2007) observed similar unstable structures produced near the roughness elements.

The vortical structures observed in Fig. 15 are formed at the trailing edge of the roughness element through the interaction of the incoming flow and the almost stagnant flow behind the roughness. This mechanism is reminiscent of that occurring in a shear layer in a backward step flow. One may argue that, similarly to a backward step flow, the interaction of the overlying flow and the flow behind the roughness element produces a shear layer, as the PLIF images suggested. However, as in the DNS of Le et al. (1997), the shear layer originates and evolves within a turbulent environment which makes the layer unstable. It is likely that the magnitude of λ/k plays a role in controlling the shear layer. Further studies should be carried out to document the characteristics of the shear layer and how it is affected by this ratio.

Figure 15 and the PLIF images clearly indicate that the roughness perturbs the bursting phenomenon, i.e., cycle of lift up, ejection and sweep (Robinson 1991; Panton 1999) responsible for the turbulence production in a smooth wall turbulent boundary layer. They imply that the turbulence production mechanism in the present turbulent boundary layer is different from that on a smooth wall. A possible scenario for the turbulence production mechanism may be as follows: unstable shear layer vortices are shed at the trailing edge of the roughness element and convected

downstream before impacting on the following roughness element. This results in an outward motion, which leads to an intermittent form drag and turbulence production. Quite interestingly and from a practical point of view, this chain of events may suggest that an effective way for reducing the drag of the rough surface might be to control the shear layer in order to reduce or eliminate the shedding of vortices. As an example, a possible control strategy would be to apply a pulsating synthetic jet at the trailing edge of the roughness elements. Such an approach has been tried in a shear layer over a backward-facing step (Pastor et al. 2006).

4 Conclusions

Particle image velocimetry (PIV) measurements and planar laser induced fluorescence (PLIF) visualizations have been made in a turbulent boundary layer over a rough wall. The wall roughness consists of square bars placed transversely to the flow at a pitch to roughness height ratio λ/k of 11 for the PLIF experiments and $\lambda/k = 8$ and 16 for the PIV measurements. The ratio between the boundary layer thickness and the roughness height k/δ is about 20 for the PLIF and 38 for the PIV.

As one may have expected, the near-wall flow, which is strongly influenced by the roughness elements, is different from that of a smooth wall. However, both the PLIF and PIV revealed the existence of quasi-coherent structures, in the form of spanwise vortices whose size is about that of the roughness elements. These structures originate at the trailing edge of the roughness elements and are convected downstream either downward or upward. There are however unstable and interact strongly with the overlying turbulent flow.

The mean flow analysis showed that a steady recirculatory motion takes place behind a roughness element whose streamwise extent varies slightly with λ/k. The streamwise mean velocity presents a downward shift which varied marginally between the two cases of λ/k, in agreement with previous measurement and DNS results. The data indicate that the Reynolds stresses normalized by the wall units are higher for the case $\lambda/k = 16$ than those for $\lambda/k = 8$ in the outer region of the flow suggesting that the roughness density effects may be felt well beyond the near-wall region of the flow.

It is argued that the turbulence production mechanism is related to the formation of shear layer vortices at the trailing edge of a roughness element and their interaction with the overlying flow. The measured turbulence production term $-\langle uv \rangle \partial U/\partial y$ would suggest that the turbulence production is correlated with the form drag.

References

Ashrafian A, Anderson HI, Manhart M (2004) DNS of turbulent flow in a rod-roughened channel. Int J Heat Fluid Flow 25:373–383

Cui J, Patel VC, Lin C-L (2003) Large-eddy simulation of turbulent flow in a channel with rib roughness. Int J Heat Fluid Flow 24:372–388

DeGraaff DB, Eaton JK (2000) Reynolds-number scaling of the flat-plate turbulent boundary layer. J Fluid Mech 422:319–346

Djenidi L, Elavarasan E, Antonia RA (1999) Turbulent boundary layer over transverse square cavities. J Fluid Mech 395:271–294

Furuya Y, Miyata M, Fujita H (1976) Turbulent boundary layer and flow resistance on the plates roughened by wires. *Trans* ASME J Fluids Eng 98:635–644

Ikeda T, Durbin PA (2007) Direct simulations of rough-wall channel flow. J Fluid Mech 571:235–263

Jimenez J (2004) Turbulent flows over rough walls. Ann Rev Fluid Mech 36:173–196

Kameda T, Mochizuki S, Osaka H (2004) LDA measurements in roughness sublayer beneath a turbulent boundary layer developed over two-dimensional square rough surface. In: Proceedings of the 12th international symposium on applications of laser techniques to fluid mechanics, paper 28–3, CD-ROM, 12–15 July, Lisbon

Kogstad P-A, Antonia RA (1999) Surface roughness effects in turbulent boundary layers. Exp Fluids 27:450–460

Kogstad P-A, Anderson HI, Bakken OM, Ashrafian A (2005) An experimental and numerical study of channel flow with rough walls. J Fluid Mech 530:327–352

Le H, Moin P, Kim J (1997) Direct numerical simulation of turbulent flow over a backward-facing step. J Fluid Mech 330:349–374

Leonardi S, Orlandi P, Smalley RJ, Djenidi L, Antonia RA (2003) Direct numerical simulations of turbulent channel with transverse square bars on one wall. J Fluid Mech 491:229–238

Leonardi S, Orlandi P, Smalley RJ, Djenidi L, Antonia RA (2004) Structure of turbulent channel flow with square bars on one wall. Int J Heat Fluid Flow 77:41–57

Panton RL (ed) (1999) Self-sustaining mechanisms of wall turbulence, advances in fluid mechanics, vol 15. Computational Mechanics Publications, Southhampton

Pastor M, Noack BR, King R (2006) Spatiotemporal waveform observer and feedback in shear layer control. AIAA paper 2006–1402

Perry AE, Schofield WH, Joubert P (1969) Rough wall turbulent boundary layer. J Fluid Mech 165:163–199

Rehab H, Djenidi L, Antonia RA (1999) LDV and PLIF measurements in a turbulent boundary layer over a rough wall. In: Proceedings of the 2nd Australian conference on laser diagnostics in fluid mechanics and combustion. Melbourne, pp 132–137

Robinson K (1991) Coherent motions in the turbulent boundary layers. Ann Rev Fluid Mech 23:601–639

Smalley RJ, Antonia RA, Djenidi L (2001) Self-preservation of rough wall turbulent boundary layer. Eur J Mech B Fluids 20:591–602

Townes HW, Sabersky RH (1966) Experiments on the flow over a rough surface. Int J Heat Mass Transf 9:729–738